ACS Biomaterials SCIENCE & ENGINEERING

pubs.acs.org/journal/abseba

Article

Multiwell Combinatorial Hydrogel Array for High-Throughput Analysis of Cell–ECM Interactions

Ruoxing Lei, Erin A. Akins, Kelly C. Y. Wong, Nicole A. Repina, Kayla J. Wolf, Garrett E. Dempsey, David V. Schaffer, Andreas Stahl, and Sanjay Kumar*

Cite This: *ACS Biomater. Sci. Eng.* 2021, 7, 2453–2465

Read Online

ACCESS | Metrics & More | Article Recommendations | Supporting Information

ABSTRACT: Biophysical cues in the extracellular matrix (ECM) regulate cell behavior in a complex, nonlinear, and interdependent manner. To quantify these important regulatory relationships and gain a comprehensive understanding of mechanotransduction, there is a need for high-throughput matrix platforms that enable parallel culture and analysis of cells in various matrix conditions. Here we describe a multiwell hyaluronic acid (HA) platform in which cells are cultured on combinatorial arrays of hydrogels spanning a range of elasticities and adhesivities. Our strategy utilizes orthogonal photopatterning of stiffness and adhesivity gradients, with the stiffness gradient implemented by a programmable light illumination system. The resulting platform allows individual treatment and analysis of each matrix environment while eliminating contributions of haptotaxis and durotaxis. In human mesenchymal stem cells, our platform recapitulates expected relationships between matrix stiffness, adhesivity, and cell mechanosensing. We further applied the platform to show that as integrin ligand density falls, cell adhesion and migration depend more strongly on CD44-mediated interactions with the HA backbone. We anticipate that our system could bear great value for mechanistic discovery and screening where matrix mechanics and adhesivity are expected to influence phenotype.

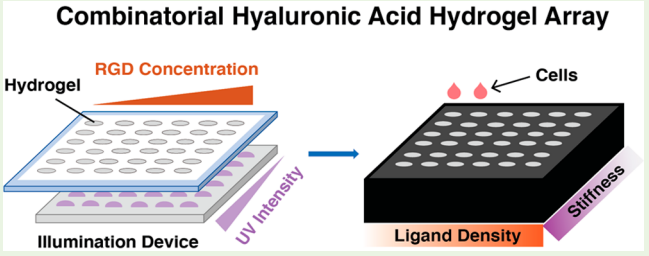

KEYWORDS: *mechanobiology, biomaterials, hyaluronic acid, combinatorial matrix arrays*

INTRODUCTION

Cells in tissue constantly sense and respond to biochemical and biophysical inputs from the microenvironment, including the extracellular matrix (ECM). Cell-ECM biophysical interactions profoundly impact many biological processes such as stem cell development,[1] tumor progression,[2,3] and immune responses.[4] The relationships between individual matrix parameters and phenotype are often complex, nonlinear, and interdependent. For example, matrix stiffness can drive cell behavior synergistically or antagonistically with adhesive ligand density, stress relaxation properties, and surface wettability.[5−7] Mesenchymal stem cell (MSC) phenotypes and transcriptomic profiles have also been reported to be nonlinearly regulated by topography and stiffness.[8−10] An important barrier to deconstructing this complex phase space has been the relative paucity of biomaterial platforms that allow for combinatorial or parallel deployment of many matrix conditions simultaneously.

Synthetic hydrogels are commonly used to mimic ECM because of their structural and mechanical similarities to native ECM and the versatility with which they can be chemically functionalized.[11−14] Synthetic hydrogel platforms have been successfully applied to investigate cellular responses to various biophysical cues such as matrix mechanics,[15−17] adhesivity,[5,18,19] and topography.[20,21] As interest has grown in understanding how matrix biophysical properties influence cell behavior, there has been much effort to engineer combinatorial hydrogel systems in which multiple ECM properties can be systematically and independently varied, analogous to experiments in which cultured cells are treated with systematic combinations of small molecules or growth factors to assess multifactorial interactions. For example, we and others have developed hydrogel platforms with dual gradients of stiffness and adhesive peptide density to investigate their coupling effects on adhesion, migration, and fate commitment.[22−24] Other examples include hydrogels with orthogonal peptide gradients, stiffness and roughness gradients, and stiffness and wettability gradients.[7,8,25,26] These high-throughput hydrogel platforms can be categorized into discrete hydrogel arrays[24,27,28] and continuous gradient hydrogels.[23,25,29] An important advantage of discrete arrays is the ability to isolate cells within a given set of matrix conditions, thereby eliminating cellular crosstalk across matrix conditions and permitting isolated extraction of cells

Received: January 14, 2021
Accepted: April 28, 2021
Published: May 24, 2021

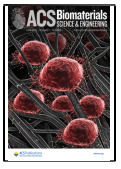

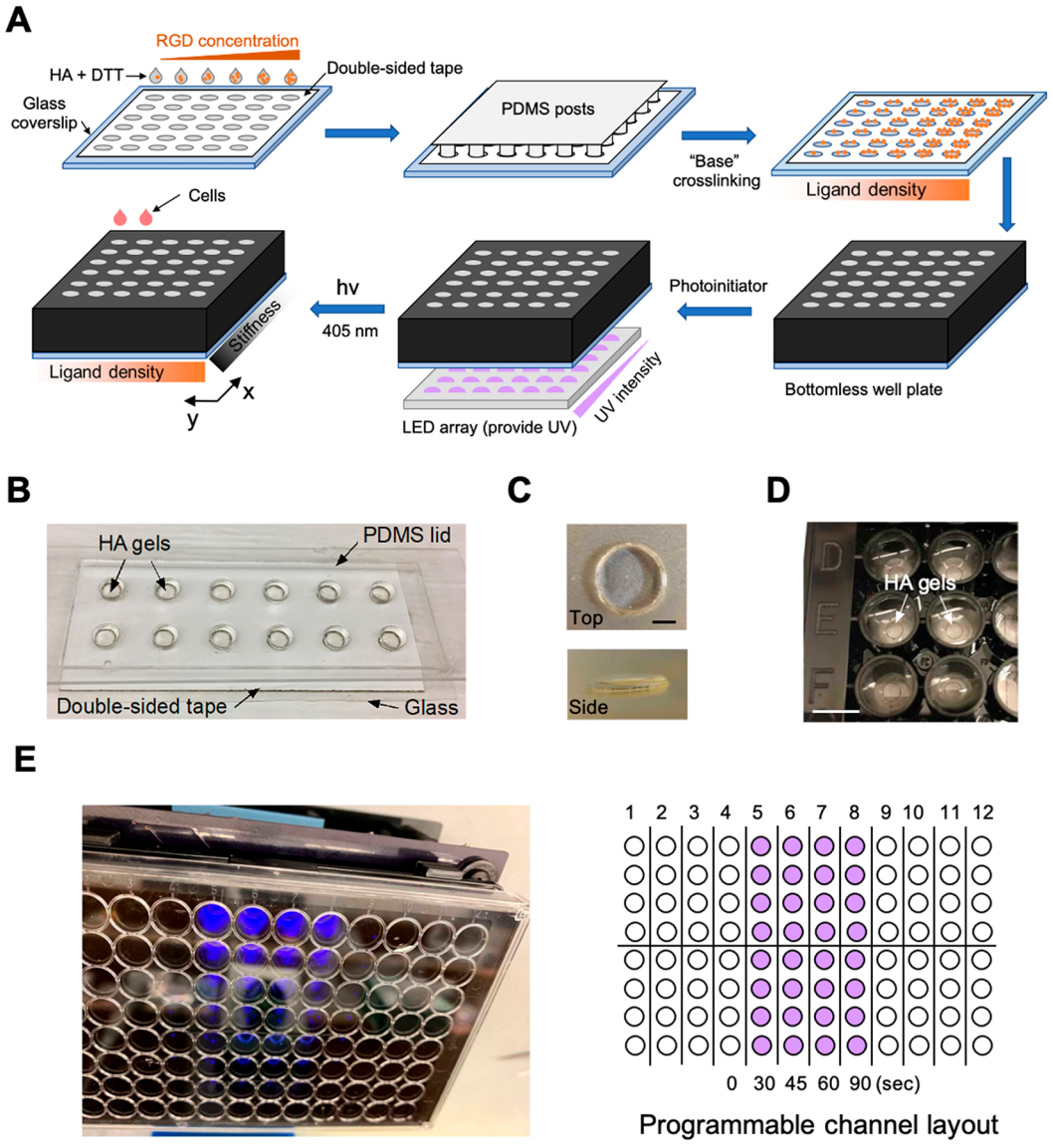

Figure 1. Fabrication of the HA hydrogel array platform. (A) Workflow of the array fabrication. RGD density is controlled by mixing 10 wt % HA-Me solutions with varying RGD peptide concentrations. Stiffness is determined by the accumulation of two cross-linking steps: first by DTT and then by radical photo-cross-linking. (B) Array in its "sandwich" assembly with PDMS lid. (C) Top view (upper) and side view (lower) of one gel in the array. Each gel is ~3 mm wide and ~200 μm thick. Scale bar: 1 mm. (D) Array assembled with a bottomless 96-well plate. Scale bar: 5 mm (E) Hydrogel array is photopatterned by a light activation at variable amplitudes (LAVA) device (left). The LAVA device can control 24 independent channels with programmable intensity and illumination time (right). Purple wells represent channels illuminated with UV light for various exposure times.

and/or media from individual matrix conditions for downstream analysis.

Matrix arrays with hundreds or even thousands of gels on one device can be fabricated using dedicated robotic spotters.[30,31] However, specialized instrumentation is needed to construct and read these arrays, and the extensive parallelization afforded by these platforms is not always required. It would also be advantageous to deploy multiplex hydrogel platforms in standard multiwell culture plate formats, for which a wealth of bioanalytical assays has been developed. Although efforts have been made to engineer multiwell gel arrays, most notably by assembling gels directly in the wells of standard culture plates,[32−34] most of these approaches have varied a single ECM parameter at a time (e.g., stiffness), and there remains a strong need for ECM platforms that can be implemented in multiwell formats where multiple matrix parameters can be varied both independently and in parallel.

Here we describe a combinatorial, multiwell hydrogel array platform in which cells are cultured on hyaluronic acid (HA) gels with combinations of stiffness and adhesive RGD peptide density. HA is a common backbone of ECM-mimetic hydrogels in tissue engineering due to its biocompatibility and flexibility to chemical modifications.[35,36] We and others have used methacrylated HA (HA-Me) hydrogels with tunable mechanical properties to study cell−matrix interactions that depend on stiffness, adhesive ligand density, topography, or other biophysical cues.[37−40] Our approach innovates upon our previously described photopatterning strategy, in which we created orthogonal, continuous gradients of stiffness and adhesive ligand density.[22] Our new platform employs discrete ECM wells, made possible by replacing the gradient photomask

https://doi.org/10.1021/acsbiomaterials.1c00065
ACS Biomater. Sci. Eng. 2021, 7, 2453−2465

with a custom-designed and programmable LED array.[41,42] As a result, our platform allows individual treatment and extraction of cells from individual matrix environments while eliminating contributions of haptotaxis and durotaxis. We conducted proof-of-principle studies with human adipose-derived mesenchymal stem cells (hMSCs) to validate this platform and recapitulated the relationships between matrix stiffness and adhesivity on hMSC morphology. We further applied this platform to investigate the coupling effects of stiffness and adhesivity on human glioblastoma (GBM) cell spreading, adhesion, and migration in the presence or absence of the HA-binding receptor CD44.

EXPERIMENTAL SECTION

Materials and Methods. *Synthesis and Characterization of Methacrylated Hyaluronic Acid.* Methacrylated HA (HA-Me) was synthesized as described previously.[37] Briefly, sodium hyaluronate (MW 66−90 kDa range; Lifecore Technologies) was dissolved at 1 wt % in deionized water, and a 10-fold molar excess of methacrylic anhydride (Sigma-Aldrich; relative to the HA disaccharide repeat unit) was added dropwise to the solution on ice. The pH was adjusted to 8−9 by 10 N NaOH and the reaction was maintained at 4 °C overnight. The next day, 2-fold molar excess of methacrylic anhydride was added dropwise to the solution. The pH was adjusted to 8−9 by 10 N NaOH and the reaction was maintained at 4 °C for another day. Afterward, methacrylated HA was precipitated from the aqueous solution by adding excess cold ethanol (Proof 200 ethanol, anhydrous, Koptec). The mixture was then centrifuged at 4000*g* to recover the precipitate, which was redissolved in deionized water, frozen at −80 °C, and lyophilized. ^{1}H NMR spectra were collected at 400 MHz using a Bruker Avance AVB-400 instrument. The degree of methacrylation was then calculated as the ratio of the vinylic protons from the methacrylate group to the N-acetyl methyl protons from the HA backbone, normalized to the number of protons per group. A methacrylate to HA monomer ratio of ∼70% was achieved (Figure S1).

Fabrication of HA Array. A lid with an array of polydimethylsiloxane (PDMS) (SYLGARDTM 184 silicone elastomer kit, Dow-Corning) posts was cast using acrylic molds. The acrylic mold was custom-made by laser-cutting and stacking 1.5 mm-thick acrylic sheets (CLAREX Precision Thin Sheet, 1.5 mm, Astra Products). Specifically, a 1.5 mm-thick acrylic sheet was perforated with a H-series 20 × 12 Desktop CO2 Laser Engraver (Full Spectrum Laser) to generate an array of 3.3 mm wide circular holes, with the distance between circles equal to the well-to-well distance of a standard 96-well plate (∼0.90 cm) (Figure S2, Sheet A). A spacer acrylic sheet (Figure S2, Sheet B) with a rectangular cutout was placed on top of Sheet A, with another rectangular acrylic sheet (Figure S2, Sheet C) at the bottom of Sheet A. PDMS was poured into the mold, a glass slide (Fisherbrand, 12-550-A3) was placed on top of Sheet B, and the sandwich assembly was clamped together with large binder clips. The PDMS was cured at 80 °C for at least 2 h before disassembling the acrylic casting mold. The lid can be "recharged" for subsequent uses with 10 min plasma treatment (Harrick Plasma, PDC-32G) immediately before each use, for up to 10 reliable reuses.

A piece of double-sided tape (ARcare 90106, Adhesives Research) was laser cut to generate an array of 3 mm-wide circular holes, with the distance between holes equal to the well-to-well distance of a standard 96-well plate. One side of the tape cover was removed, and the tape was affixed to a No. 1.5 cover glass (Ted Pella, product 260423; 260461-100). Most experiments performed in this manuscript utilized a 24 (or 36) × 60 mm cover glass rectangle; however, the glass may be cut to smaller dimensions using a pen-style glass cutter to accommodate the dimensions of customized gel arrays. A 1 mg/mL poly-D-lysine (PDL, MW > 300 000, Sigma-Aldrich) solution was used to coat the glass for 1 min followed by a 2 × 1 min rinse in double-distilled H_2O to facilitate HA hydrogel attachment.

HA-RGD precursor solutions were made by mixing appropriate volumes of 10 wt % HA-Me, 4 mg/mL reconstituted RGD adhesive peptide (Ac-GCGYGRGDSPG-NH2, Anaspec), and 1× PBS and then vortexing at room temperature for at least 1 hour. The final HA-RGD precursor solutions had 5.71 wt % HA-Me but varying RGD conjugation concentrations. HA-RGD precursor solutions were mixed with 5 wt % dithiothreitol (DTT, Thermo Fisher Scientific) and 1× PBS to achieve a 0.15 thiol to HA repeat unit ratio (T/H ratio) and a final 5 wt % HA-Me. The hydrogel solution (4.8 μl per gel) was immediately pipetted onto the PDL-treated glass surface (Figure 1A). The PDMS lid was then placed on top of the coverslip to form a sandwich assembly (Figure 1B). The assembly was allowed to sit at room temperature in a moisturized chamber overnight for hydrogel cross-linking. The following day, the assembly was soaked in 1× PBS for at least 10 min to detach the PDMS lid from the gel array. The double-sided tape cover was removed, and the newly exposed adhesive surface was used to adhere the gel array onto a bottomless 96-well black-wall culture plate (Greiner Bio-One International GmbH, #82051−528), and the plate was then covered with a 96-well lid (Evergreen Scientific, 290-8019-01L) (Figure 1C, D). When soaked in sterile 1× PBS, the gel array can be stored at 4 °C for up to one week. For cell differentiation assays and other long-term (>1 day) cell culture studies, sterile PBS was used at all times, plastic culture supplies were disinfected by UV radiation and the fabrication process occurred in a biosafety hood to minimize microbial contamination.

Stiffness Gradient Patterned by a Programmable Light Illumination System. A specialized illumination device for light activation at variable amplitudes (LAVA) was used for gel photostimulation (Figure 1E). The LAVA device was designed for 96-well plate illumination as described previously.[41,42] Briefly, the illumination intensity of a surface-mount 405 nm LED (SMT405R, Marubeni) placed at the center of each well was controlled with pulse-width modulation. User-defined intensities for each well were programmed through a graphical user interface to allow 405 nm illumination in the [0−33.5] $\mu W/mm^2$ intensity range. The LAVA device allowed independent control of 24 channels, so that clusters of four vertical wells were controlled simultaneously in the 96-well format (Figure 1E).

Lithium phenyl-2,4,6-trimethylbenzoylphosphinate (LAP, Allevi) was dissolved in 1× PBS to make a 0.5 wt % solution. Freshly made LAP solution (100 μL) was added to each well and the gels were incubated on a shaker for 1 h at room temperature. The array was then placed on the LAVA device and exposed to 405 nm UV light (intensity measured at the center of hydrogel = 15 $\mu W/mm^2$) for various amounts of time programmed by previously described software.[41] Afterward, the LAP solution was immediately removed and the array was washed with 1× PBS for 2 × 10 min on a shaker to remove excess LAP.

Atomic Force Microscope Characterization of Hydrogel Array. For AFM measurements, the hydrogel array was first attached to a removable plastic chamber that held the LAP solution during photo-cross-linking on the LAVA device. Afterward, the LAP solution was replaced with 1× PBS. AFM was performed with a Veeco Catalyst Bioscope (Bruker Corporation, Camarillo, California, USA). The gels were indented using a pyramid-tipped probe (DNP-10, Bruker AFM Probes) with cantilever spring constants of 0.12−0.24 N/m, as measured by thermal calibration. Typically, five force curves per hydrogel were collected at different positions at least 100 μm apart from each other. Elastic moduli of the gels were calculated from force curves using a modified Hertz model, as previously described.[43]

Cell Culture. Human primary adipose-derived mesenchymal stem cells (hMSC) were purchased from ATCC (PCS-500-011) and maintained and grown in accordance with the manufacturer's recommendations. Cells were cultured in hMSC growth medium with corresponding growth supplements (ATCC, PCS-500-040) and used at passage number <8. U-87 MG human glioblastoma (GBM) cells were obtained from the University of California, Berkeley Tissue Culture Facility, which sources its cultures directly from ATCC. U-87 MG cells were cultured in DMEM (Thermo Fisher Scientific), 1% (v/v) MEM nonessential amino acids (Thermo Fisher Scientific), and 1% (v/v) sodium pyruvate (Thermo Fisher Scientific). Cells were passaged every 5 days using 0.25% trypsin-EDTA (Thermo Fisher Scientific) and used at passage number <30. Cells were screened on a monthly basis for mycoplasma and authenticated every six months by Short Tandem Repeat (STR) analysis at the University of California Cell Culture

https://doi.org/10.1021/acsbiomaterials.1c00065
ACS Biomater. Sci. Eng. 2021, 7, 2453−2465

Facility. We used our previously developed CD44 knockout (KO) and nontargeting (NT) U-87 MG cell lines, generated using CRISPR-based gene editing.[44]

hMSC Spreading Assay and Immunostaining. hMSCs were seeded on the hydrogel array at a density of 5000−7500 cells/cm^2 and allowed to attach and grow for 16−20 h. Cells were then fixed with 4% paraformaldehyde (PFA, Sigma-Aldrich) in 1× PBS for 15 min at room temperature, permeabilized with 0.5% (v/v) Triton X-100 (EMD Millipore, 9410) in 1× PBS for 15 min at room temperature, and blocked using 5% (v/v) goat serum (Thermo Fisher Scientific) in 1× PBS for 1 hour at room temperature. YAP was visualized using YAP (D8H1X) XP rabbit monoclonal antibody (Cell Signaling Technology). Actin filaments were visualized using AlexaFluor-546 labeled phalloidin (Thermo Fisher Scientific). Cell nuclei were visualized using 4′,6-diamidino-2-phenylindole dihydrochloride (DAPI, Sigma-Aldrich). Fluorescence imaging was performed on a Nikon Eclipse Ti-E epifluorescence microscope. YAP nucleus/cytoplasm (nuc/cyto) intensity ratio was measured as the average intensity of YAP signal inside the nucleus divided by the average intensity of an area adjacent to the nucleus region, of similar size as the nucleus. Morphometric analysis of projected cell area was performed by thresholding the phalloidin fluorescence images to define the cell boundaries and applying automated particle shape analysis in *ImageJ*. Cells in clumps or near the outer edge of the gel were excluded from analysis.

hMSC Differentiation and Staining. hMSCs were seeded on the HA hydrogel array at a density of 20000 cells/cm^2 and allowed to grow in expansion medium for 1 day. Cells were then shifted to a mixed differentiation medium, consisting of a 1:1 mixture of osteogenic and adipogenic differentiation media (StemPro kits, Thermo Fisher Scientific). Cells were maintained for 7 days in mixed differentiation medium with medium change every 3−4 days.

Adipogenic differentiation of PFA-fixed hMSCs was assessed by lipid droplet staining of BODIPY 493/503 (4,4-difluoro-1,3,5,7,8-pentamethyl-4-bora-3a,4a-diaza-s-indacene, Invitrogen), at a 2 μM working concentration. The cells were then washed extensively with PBS prior to epifluorescence imaging. Osteogenic differentiation of fixed and permeabilized hMSCs was assessed by alkaline phosphatase activity using the SigmaFast BCIP/NBT assay (Sigma-Aldrich). A working solution of BCIP/NBT was prepared as per manufacturer's instructions, added to the cells, incubated for 15 min at room temperature, and then washed extensively in 1× PBS. Alkaline phosphatase staining was identified as a dark purple color and imaged on an Olympus IX50 inverted fluorescence phase contrast microscope, with images captured by a Canon EOS Rebel T3 digital SLR camera.

U-87 Cell Spreading Assay. Cells were harvested and seeded onto HA gel arrays at a density of 6000 cells/cm^2 and incubated for at least 6 h. Cells were imaged using a 10× UPLFN objective lens and the MuviCyte Live-Cell Imaging System (PerkinElmer, Massachusetts, USA) in a 37 °C, CO_2 controlled chamber. At least 20 cells were randomly selected for cell spreading quantification. Cells in multicellular clusters or near the outer edge of the gel were excluded from analysis. Cells with zero visible protrusions when viewed with a 10× objective were labeled as "round" while cells with one or more protrusions were labeled as "spread."

U-87 Centrifugal Adhesion Assay. A centrifugal adhesion assay was performed based on our previously reported protocol.[38,44] Briefly, cells were harvested and seeded onto HA gels at a density of 6000 cells/cm^2 and incubated for at least 6 h. Prior to centrifugation, wells were filled with the addition of fresh medium, and cell culture plates were sealed with an adhesive plate sealer (Microseal 'B' Adhesive Seals, BioRad). The plate was then inverted and centrifuged for 5 min at 100*g*. Following centrifugation, media was removed from the wells and cells remaining on hydrogels were fixed by PFA and stained with DAPI. Images were captured using the MuviCyte Live-Cell Imaging System. At least three unique microscopic fields were randomly imaged per well using a 10× objective lens. Automated thresholding analysis of the DAPI images was performed on *ImageJ* to determine a total count of the number of cells in each field of view.

U-87 Migration Assay. Cells were seeded onto HA gels at a density of 6000 cells/cm^2 and incubated for at least 6 h. Then, migration assays were performed by imaging cells at 15 min intervals for 8 h using the Muvicyte Live-Cell Imaging System with a 10× objective in a 37 °C, CO_2 controlled chamber. The *ImageJ* Manual Tracking plug-in was used to track cell movements in each frame and calculate an average cell speed. Cells that were dividing, in multicellular clusters, or near the outer edge of the gel were excluded from analysis.

Real-Time Polymerase Chain Reaction (RT-PCR). Prior to cell seeding, a ring-shaped tape cover was laser cut from the double-sided tape and adhered to the bare tape region in each well of the gel array. Cells were then seeded onto the array and allowed to differentiate as described above. At the conclusion of the differentiation assay, the tape cover and all cells attached to the cover was removed by tweezers, whereas only cells attached to the hydrogels remained in the wells. Cells were then lysed and RNA was extracted following the manufacturer's protocol (ReliaPrep RNA Miniprep systems, Promega Corporation). cDNA was synthesized using qScript cDNA SuperMix (Quantabio) following the manufacturer's protocol. Real-time PCR reactions were prepared with a SYBR Green qPCR Master Mix (Bimake) and the PCR cycle was performed on a BioRad CFX Connect Real-Time System.

The following primer sequences were used in RT-PCR of hMSCs: ALP (ACC ACC ACG AGA GTG AAC CA; CGT TGT CTG AGT ACC AGT CCC, Elimbio), FABP4 (ACG AGA GGA TGA TAA ACT GGT GG; GCG AAC TTC AGT CCA GGT CAA C, Genewiz), and GAPDH (GTC AAG GCT GAG AAC GGG AA; AAA TGA GCC CCA GCC TTC TC, Elimbio).

Quantification and Statistical Analysis. Statistical significance was calculated by the indicated tests using GraphPad/Prism, and statistical details can be found in figure legends. For figures in which multiple comparison analysis are displayed by letters, conditions with a common letter are not significantly different according to the stated statistical test at the 5% level of significance ($p < 0.05$).

RESULTS

HA Hydrogel Array Fabrication and Characterization.

Our hydrogel array platform is assembled by casting HA hydrogel precursors in two-dimensional array patterns on a glass substrate that is later affixed to a bottomless multiwell plate. This fabrication method results in individually accessible wells, each containing a single gel. Key to this approach is the use of laser-cut double-sided tape, which serves both as a template for casting the HA gel solution and as an adhesive to affix the glass to the bottomless multiwell plate. We began array fabrication by using a laser cutter to perforate the double-sided tape to generate a two-dimensional array of circular holes corresponding to the desired dimensions and distribution of gels. We then exposed one adhesive side of the patterned double-sided tape in order to attach the patterned tape to an appropriately sized glass coverslip, also refered to as the cover glass. HA-RGD hydrogel precursors were mixed with DTT and then pipetted into the shallow "wells" formed by the union of the patterned double-sided tape and the glass surface (Figure 1A). A lid of PDMS posts was immediately applied to flatten gel interfaces during initial cross-linking (Figure 1B). The resulting hydrogels are ∼200 μm thick, approximately the same thickness as the double-sided tape, and 3 mm wide, approximately the same diameter as the circular holes patterned in the double-sided tape (Figure 1C). Following gelation and removal of the PDMS lid, the top adhesive surface of the tape was exposed and used to adhere the glass to a bottomless multiwell plate (Figure 1D). The bottomless well plate, double-sided tape, and glass formed a tight seal that prevented media leakage and exchange between neighboring wells (Figure S3). For this study, we designed the array in a 96-well plate format, but the fabrication technique can be readily adapted to other plate types (e.g., 6-, 12-, 24-well) by customizing the dimensions of the patterned double-sided tape and PDMS lid.

https://doi.org/10.1021/acsbiomaterials.1c00065
ACS Biomater. Sci. Eng. 2021, 7, 2453−2465

The array platform varies elasticity across wells in the *x*-direction and independently varies adhesive ligand density (adhesivity) along wells in the *y*-direction (Figure 1A). Prior to cross-linking, we conjugated various concentrations of RGD peptide (GCGYGRGDSPG) to HA-Me precursors (Figure S1) through thiol−ene reactions, generating RGD-modified HA (HA-RGD) precursors with varying RGD densities. HA-RGD precursors then underwent a two-step cross-linking reaction to generate the stiffness gradient. In the first step, HA-RGD was mixed with DTT at a thiol to HA unit ratio (T/H ratio) of 0.15 to create a relatively soft "base" gel. The second cross-linking step involved a tunable illumination process using a previously developed device featuring light activation at variable amplitudes (LAVA).[41,42] On the LAVA device, individual hydrogel-containing wells were irradiated with a programmable 405 nm LED in the presence of LAP photoinitiator (Figure 1E). In our study, we illuminated the gel with a UV intensity of 15 μW/mm^2 and adjusted the illumination time to achieve varying levels of cross-linking.

To characterize the stiffness gradient generated by the two-step cross-linking reaction we used atomic force microscopy (AFM). Young's moduli were extracted by fitting the resulting force−indentation curves to a Hertz model, as described previously.[43] Hydrogel stiffness was highly correlated with illumination time, spanning a dynamic range of 12 to 91 kPa with 0 to 90 seconds of LED illumination (Figure 2). An extended illumination time can increase the modulus to above 200 kPa (data not shown). Unless specified otherwise, the following studies utilized gel arrays within the 12−91 kPa range to mirror the modulus of most human tissues, which falls between 500 Pa and 100 kPa.[45,46] As illumination time increased, we observed a broader distribution of moduli across gels of a given formulation, indicating increasing heterogeneity in cross-linking. We have previously observed that HA hydrogels in this stiffness range exhibit relatively modest stiffness-dependent variations in mesh size, indicating that swelling does not appreciably alter the effective concentration of HA monomers.[37] There was no significant difference in modulus between HA-RGD gels and bare HA gels under the same illumination condition (Figure S4), suggesting that the HA backbone retained sufficient unreacted methacrylate groups after RGD conjugation for the two-step cross-linking process.

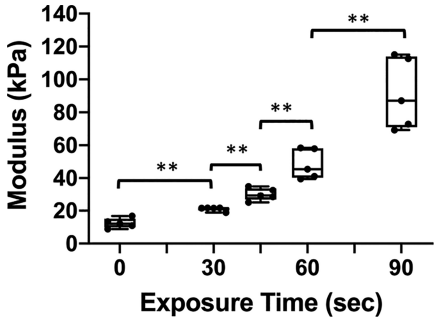

Figure 2. Stiffness gradient on the HA hydrogel array after LAP-induced photo-cross-linking of "base" 5 wt % HA-me gels with 0.5 mM RGD. Intensity of 405 nm UV radiation was fixed at 15 μW/mm^2. Gels were indented with a pyramid-tipped AFM probe and elastic moduli were calculated from at least 5 different locations on each individual gel to obtain an average elastic modulus per gel. For each condition, five individual gels were fabricated and measured in independent experiments (n = 5). After 0, 30, 45, 60, and 90 seconds of radiation, the gel modulus (mean ± standard deviation (SD)) are 12 ± 3 kPa, 21 ± 1 kPa, 30 ± 4 Pa, 48 ± 9 kPa, and 91 ± 22 kPa. All values were rounded to the nearest kPa. Statistical significance between neighboring conditions was evaluated using unpaired t tests (**p < 0.01). Boxes represent 25th and 75th percentiles and whiskers represent min and max.

Stiffness and Ligand Density Interact to Modulate hMSC Mechanosensing and Morphology. To demonstrate that our hydrogel array platform can recapitulate the effects of ECM stiffness and adhesive ligand density on cell morphology and mechanotransduction, we cultured hMSCs on our platform and evaluated cell spreading and Yes-Associated Protein (YAP) localization. YAP is a transcriptional coactivator that localizes to the nucleus under mechanical tension, where it interacts with cofactors to regulate the expression of a variety of target genes.[47,48] Specifically, YAP has been reported to preferentially localize to the nucleus of hMSCs cultured on stiff matrices but remain cytoplasmic for hMSCs on soft matrices. YAP nuclear localization has also been reported in cells cultured on matrices containing high ligand density, consistent with the notion that stiffness and ligand density can act synergistically to regulate cytoskeletal and focal adhesion assembly.[49] hMSC morphologies are also highly sensitive to matrix stiffness and adhesive ligand density in vitro.[18,50,51] We hypothesized that on our platform, increased stiffness and ligand density would enhance YAP nuclear localization and increase cell area.

To evaluate hMSC sensitivity to stiffness and RGD density, we made a 3 × 5 array with three RGD densities (0.1, 0.25, and 0.5 mM RGD in the HA-RGD precursors) and five elasticities (12, 21, 30, 48, and 91 kPa). hMSCs were seeded onto the array platform and allowed to attach for 16−20 h. The time window was chosen to ensure adequate cell attachment while minimizing interference resulting from cell division. After cell fixation and permeabilization, YAP localization was characterized by immunostaining. Cell shape and area were evaluated by phalloidin staining of the F-actin cytoskeleton. We excluded clustered cells from our analysis to minimize confounding effects of cell−cell interactions.

As expected, YAP localization was significantly affected by hydrogel stiffness and RGD density (Figure 3A−C). Stiff gels and high-RGD gels promoted YAP nuclear localization, shown as an overlap of YAP and DAPI staining (Figures 3A and Figure S5). We quantified YAP nuclear/cytoplasmic (nuc/cyt) ratio for each individual cell by calculating the ratio of the average YAP intensity in the nucleus region and the average intensity in the cytoplasmic region of similar size that is adjacent to the nucleus. Some cells, especially those on soft gels with low RGD density, had rounded morphologies that made it challenging to discern the cytoplasm from the nucleus. These cells were thus excluded from the nuc/cyt ratio analysis. As stiffness increased from 12 to 91 kPa, YAP nuc/cyt ratio increased significantly on both low RGD and medium RGD gels (Figure 3B). On gels with high RGD density, although statistical differences between low and high stiffness still persisted, the gaps in their median values were narrowed. When stiffness was below 48 kPa, YAP showed a trend to enrich in the nucleus as RGD density increased (Figure 3C). On 91 kPa gels, however, YAP localization was not sensitive to ligand density changes.

Further, hMSC spreading generally increased as stiffness and RGD density increased, along with the assembly of increasingly prominent stress fibers (Figure 4A). Stiffness-dependent spreading was seen on all three RGD densities (Figure 4B) and ligand density-dependent spreading was observed across all

https://doi.org/10.1021/acsbiomaterials.1c00065
ACS Biomater. Sci. Eng. 2021, 7, 2453−2465

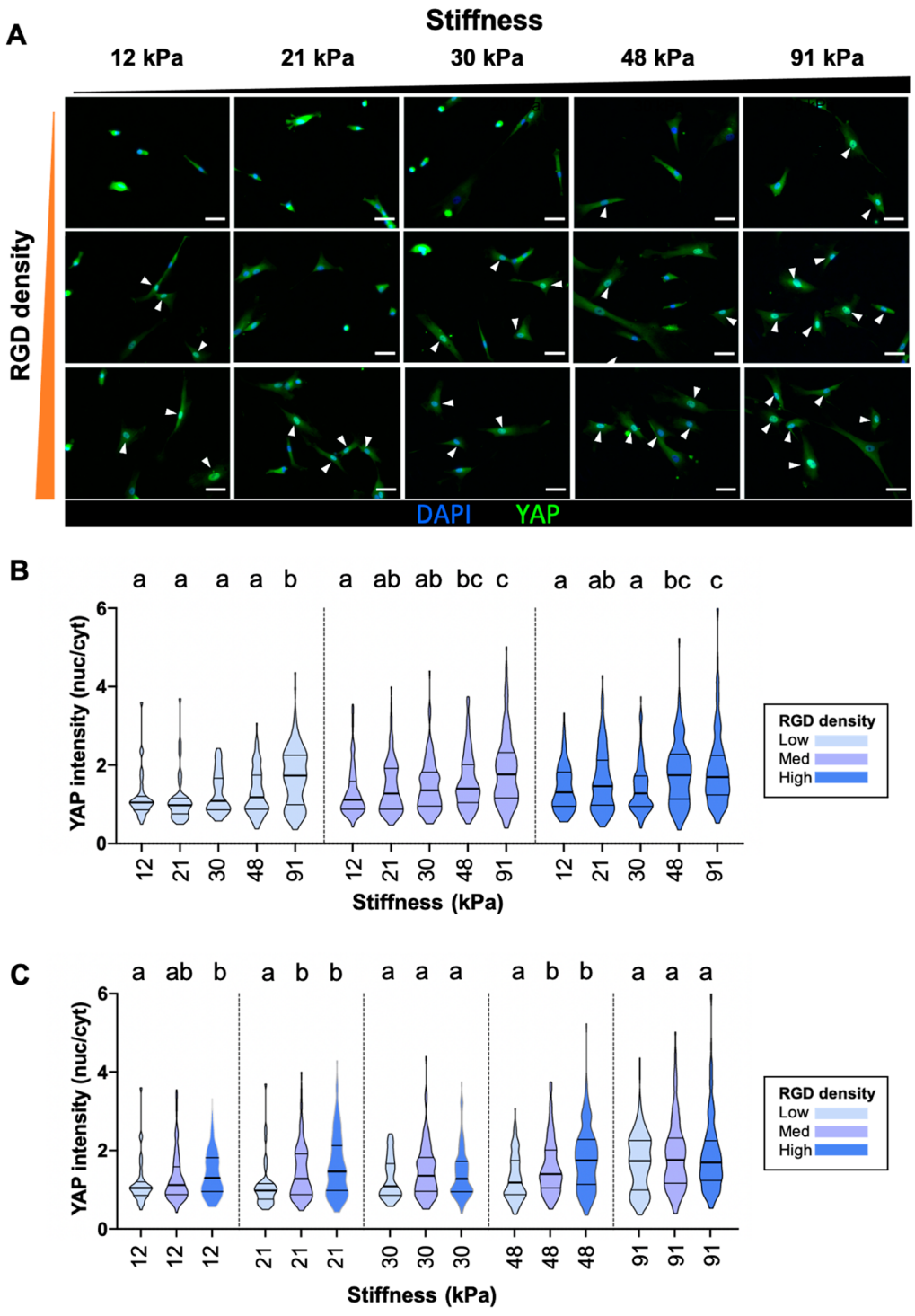

Figure 3. YAP localizes to hMSC nucleus as matrix stiffness and RGD density increase. (A) High stiffness and high RGD density promotes YAP nuclear localization. The nucleus is visualized with DAPI (blue). White arrow heads highlight cells with YAP nuc/cyt > 1.0. Scale bars: 50 μm. (B) Violin plot of YAP nuc/cyt ratios of individual cells on the array, grouped by RGD density. For each matrix condition, data was pooled from three independent experiments, as no systematic difference was observed among the triplicates. At least 40 cells were analyzed per matrix condition in each independent experiment, except on some low RGD density or soft conditions where the overall number of hMSCs attached was under 40. (C) Violin plot of the same data set as panel B, grouped by stiffness. Statistical families a, b, and c show $p < 0.05$ from Kruskal−Wallis test for multiple comparison of non-normally distributed data followed by Dunn's multiple comparisons. N equals to the total number of cells in the data set. Horizontal lines represent Q_1−Q_3.

stiffness conditions (Figure 4C). Cell area is most sensitive to stiffness at lowest RGD density. As has been observed previously, ECM stiffness and ligand density synergistically facilitate hMSC spreading.[5,22,23] Thus, the array platform successfully recapitulates expected effects of ECM stiffness and adhesivity on YAP localization and cell spreading.

https://doi.org/10.1021/acsbiomaterials.1c00065
ACS Biomater. Sci. Eng. 2021, 7, 2453−2465

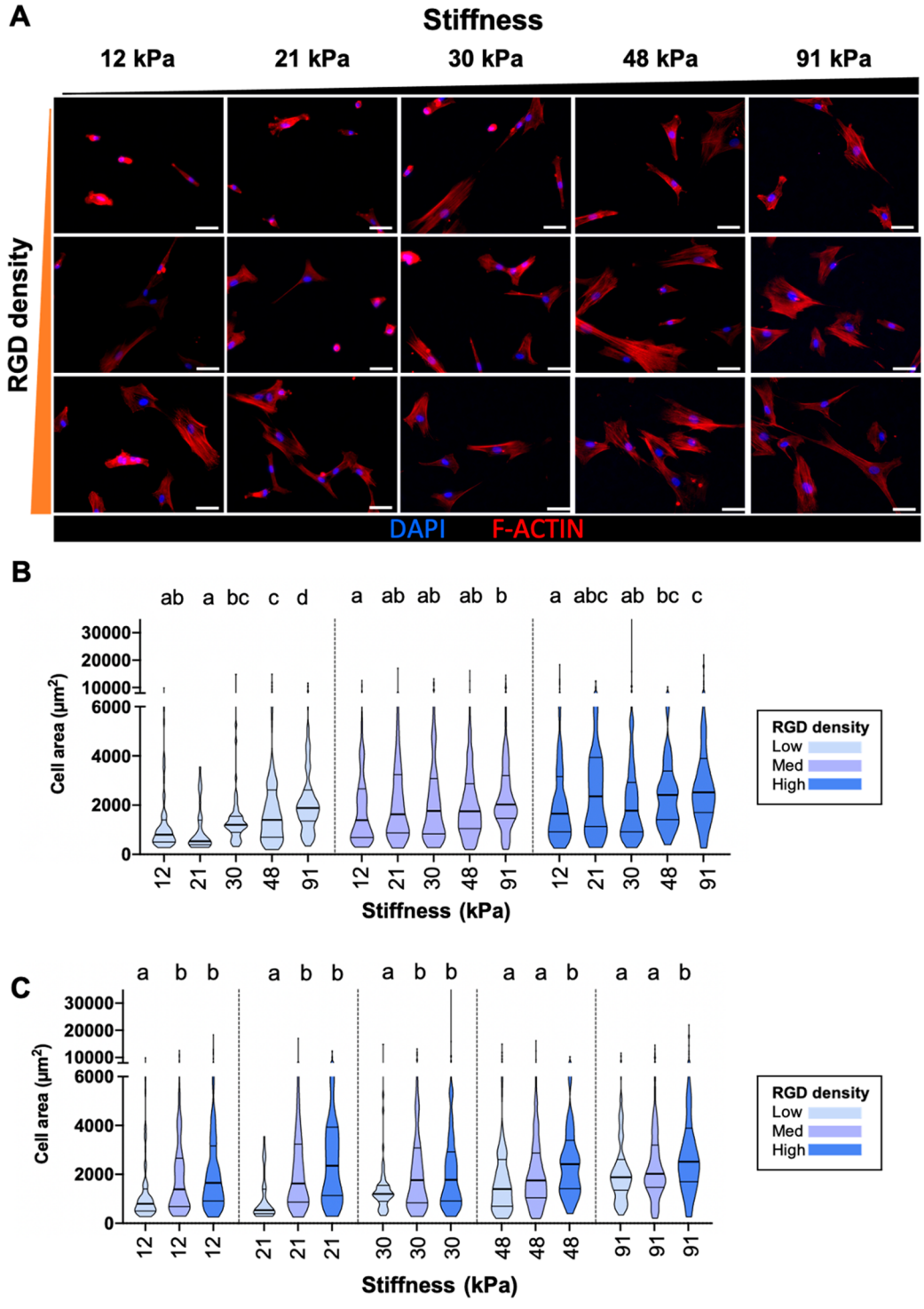

Figure 4. hMSC spreading area increases as matrix stiffness and RGD density increase. (A) High stiffness/high RGD density promotes hMSC spreading. The F-actin network is visualized with phalloidin (red) and the nucleus is visualized with DAPI (blue). Scale bars: 50 μm. (B) Violin plot of cell area (μm^2) of individual cells on the array, grouped by RGD density. For each matrix condition, data was pooled from 3 independent experiments, as we did not observe systematic difference between the triplicates. At least 40 cells were analyzed per matrix condition for each independent experiment, except on some low RGD density or soft conditions where the overall number of hMSCs attached was under 40. (C) Violin plot of the same data set as panel B, grouped by stiffness. Statistical families a, b, c and d show $p < 0.05$ from Kruskal−Wallis test for multiple comparison of non-normally distributed data followed by Dunn's multiple comparisons. *N* equals the total number of cells in the data set. Horizontal lines represent Q_1−Q_3.

Human Mesenchymal Stem Cell Differentiation on the Array. We next asked if stiffness and RGD density gradients on the array platform could direct mechanosensitive hMSC lineage commitment. It has previously been observed that hMSCs have a strong tendency to differentiate into adipocytes on soft matrices, whereas stiff hydrogels largely promote osteogenesis.[15,52−54] Using a gradient HA hydrogel with varying stiffness and fibronectin density, we also previously demon-

https://doi.org/10.1021/acsbiomaterials.1c00065
ACS Biomater. Sci. Eng. 2021, 7, 2453−2465

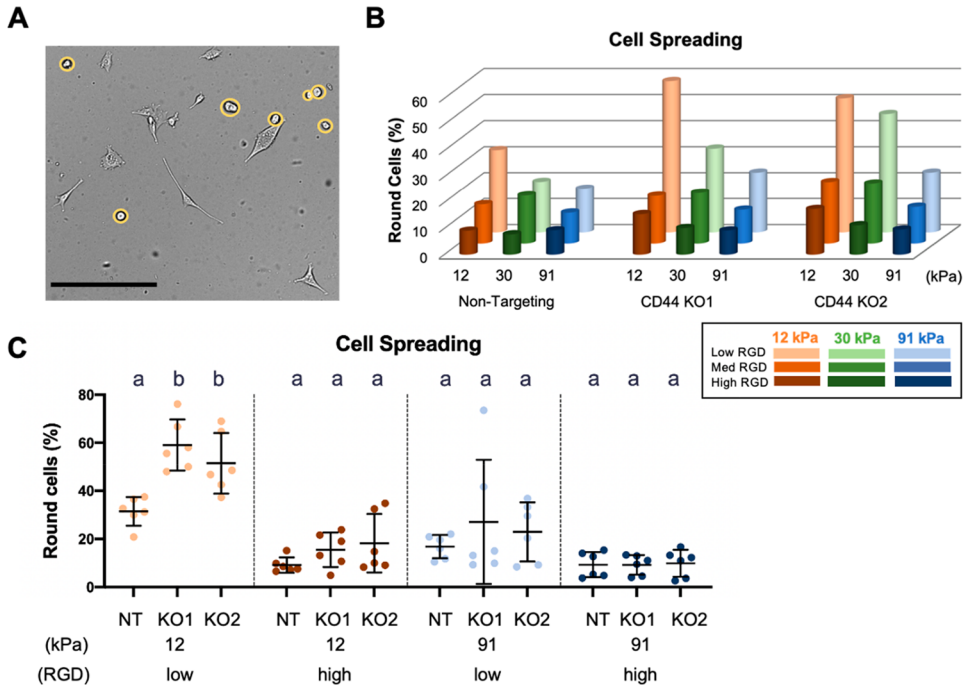

Figure 5. U-87 cell spreading increases with increasing RGD density and stiffness. (A) Representative phase image of U-87 cells on HA hydrogels. Yellow circles outline "round" cells with no visible protrusions when imaged using a 10× objective. Scale bar: 100 μm. (B) 3D column bar graph of U-87 cell spreading on HA hydrogels of varying stiffness and RGD density. Six fields of view were analyzed across three independent experiments ($n = 6$). (C) Cell spreading quantification for U-87 cells on HA hydrogels, a subset of the data set presented in Figure 5B. Statistical families a and b show $p < 0.05$ from ANOVA followed with Tukey−Kramer multiple comparisons test. Black horizontal lines represent mean and SD. (NT: nontargeting).

strated that soft, low fibronectin density matrices biased hMSCs toward adipogenesis, whereas stiff, high fibronectin density matrices supported osteogenesis.[22] We therefore hypothesized that a similar trend would be observed on this multiwell array platform.

We first evaluated whether the array was permissive for hMSC adipogenesis and osteogenesis in the presence of the corresponding induction media. We exposed the cells to a 1:1 mixture of adipogenic and osteogenic differentiation media. After 7 days of differentiation, we analyzed adipogenesis and osteogenesis by quantifying lipid droplet area and alkaline phosphatase activity, respectively. On low and medium density RGD gels, despite initial cell attachment and spreading, the majority of hMSCs migrated to form cell clusters (Figure S6A), suggesting that cell−cell interactions may be compensating for reduced matrix adhesion. We did not observe cell migration-driven clustering on high RGD gels. The 1:1 mixed induction medium induced both lineages simultaneously. Surprisingly, we did not see a strong stiffness-dependence of either adipogenic or osteogenic efficiency from 12 to 91 kPa on high RGD gels. Similar lipid droplet area and osteogenesis ALP activity were found on all stiffness conditions (Figure S6B, C). We also observed large variations in adipogenesis across experimental replicates despite consistent gel fabrication (Figure S6B). Such batch-to-batch variation may reflect the heterogeneity of hMSCs in their differentiation potency. We also measured expression levels of adipogenesis marker FABP4 and osteogenesis marker ALP across the stiffness range but did not see any stiffness-dependence in gene expression (data not shown).

Stiffness and Ligand Density Coupled to Modulate U-87 Mechanosensing and Morphology. We have previously shown that U-87 MG GBM cells adhere to HA matrices via CD44 and that this interaction becomes an increasingly important mechanism of adhesion on matrices with low RGD density.[44] Furthermore, we have shown that CD44/HA adhesion is intrinsically sensitive to matrix modulus.[38] While both HA-CD44 binding and integrins serve as important elements of mechanical control, the interaction between these two signaling pathways and their influence on cell behavior remains poorly understood. Using our HA gel array, we systematically investigated the effects of stiffness and RGD density on cell phenotype and migration to further explore the interplay between HA matrix stiffness and RGD ligand concentration on U-87 cell behavior. We hypothesized that increased stiffness and RGD density would synergistically increase GBM cell spreading, adhesion, and motility. We also hypothesized that cells lacking CD44 would display a decreased ability to attach, spread, and migrate on 2D HA hydrogels and that this phenotype could be rescued on matrices with high stiffness and high RGD density.

To investigate the role of CD44 in GBM cell sensitivity to stiffness and RGD density, we fabricated a 3 × 3 array with three different RGD densities (0.02, 0.15, and 0.5 mM RGD in the HA-RGD precursors) and three different elasticities (12, 30, and 91 kPa). We utilized our previously generated CD44 KO and nontargeting U-87 cells.[44] We seeded U-87 cells onto the array platform and performed phase imaging to observe GBM cell morphology on HA hydrogels of varying stiffness and RGD density. Cell spreading was indirectly quantified by counting the number of round cells, which we defined as cells exhibiting a circular morphology and lacking visible protrusions when imaging with a 10× phase objective (Figure 5A). CD44 KO cells generally had a higher percentage of round cells compared to nontargeting cells across all HA hydrogels, supporting the hypothesis that CD44 supports cell spreading on HA-based matrices. As we hypothesized, increasing stiffness and/or RGD

https://doi.org/10.1021/acsbiomaterials.1c00065
ACS Biomater. Sci. Eng. 2021, 7, 2453−2465

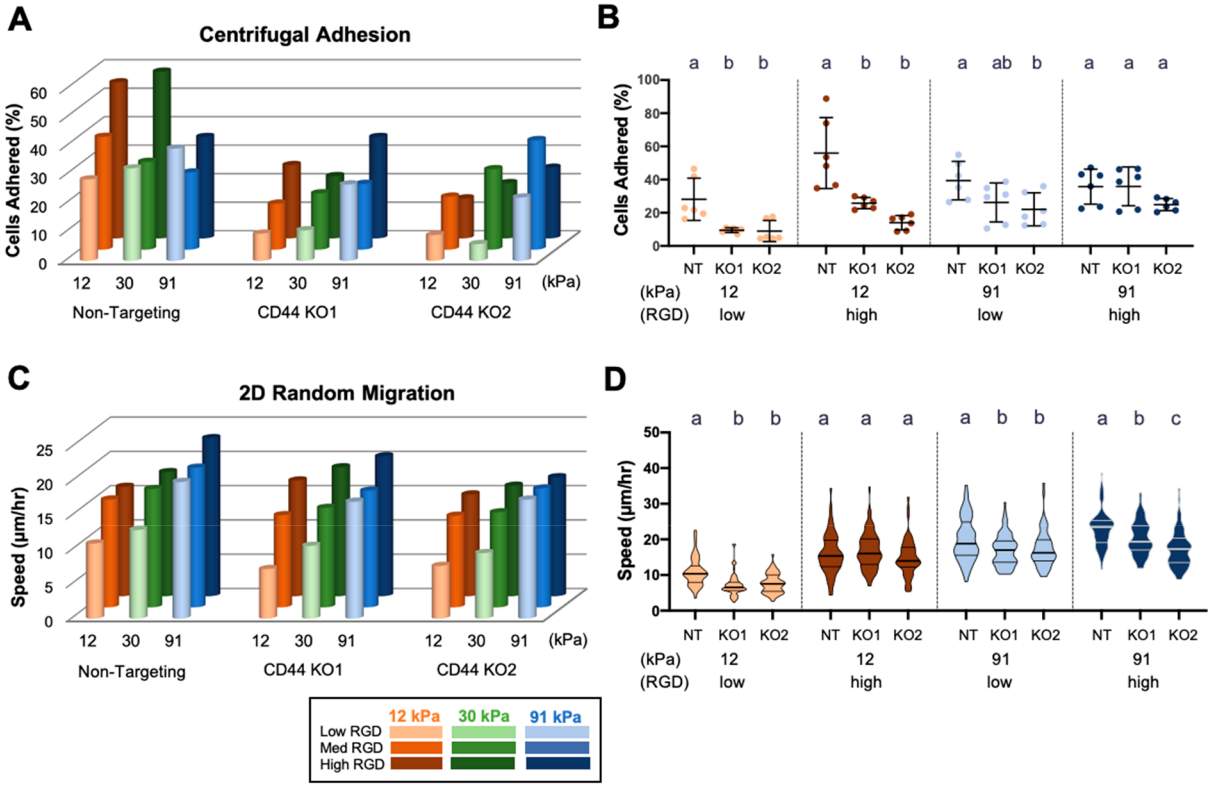

Figure 6. Cell adhesion and migration depend on HA hydrogel stiffness, RGD density, and CD44 expression. (A) 3D column bar graph of centrifugal adhesion assay for U-87 cells interacting with HA hydrogels of varying stiffness and RGD ligand density (n = 6). (B) Centrifugal adhesion assay quantification for U-87 cells on HA hydrogels. Six total fields of view were analyzed across three independent experiments (n = 6). Black horizontal lines represent mean and SD. Statistical families a and b show $p < 0.05$ by ANOVA followed by Tukey−Kramer multiple comparisons test. (C) 3D column bar graph showing 2D random migration speeds of U-87 cells on HA hydrogels with varying stiffness and RGD density (n = 60). (D) 2D random migration speeds of U-87 cells on HA hydrogels. 60 total cells were analyzed from three independent experiments (n = 6). Statistical families a, b, and c show $p < 0.05$ by Kruskal−Wallis test for multiple comparison of non-normally distributed data followed with Dunn's multiple comparisons. Horizontal lines represent Q_1−Q_3. (NT: nontargeting).

density was associated with a decreasing percentage of round cells in both nontargeting and CD44 KO cells (Figure 5B and Figure S7). Interestingly, on 12 kPa hydrogels, the CD44 KO cell population contained significantly more round cells than the nontargeting population on gels with low RGD density but had a similar fraction of round cells on gels with high RGD density (Figure 5C). There were no differences in the percentage of round cells across cell types on the stiffest gels, regardless of RGD density, suggesting that CD44-mediated signaling may influence cell spreading on soft matrices and conditions with low RGD density more than on stiff hydrogels or in conditions with high RGD density.

U-87 Adhesion on Soft HA Matrices is Enhanced by CD44-HA Binding. To more directly test the role of CD44 in facilitating cell attachment on HA matrices of varying stiffness and RGD density, we measured cell adhesion on our gel array using a previously established centrifugal adhesion assay.[38,44] We found that CD44 KO cells displayed reduced adhesion compared to nontargeting cells across all gel conditions, with 30 kPa high RGD and 91 kPa high RGD gels as the two exceptions (Figure 6A and Figure S8). In contrast to the cell spreading trends, increasing RGD density did not rescue adhesion in the CD44 KO cells on soft gels (Figure 6B). Increasing RGD density on stiff gels, however, did rescue adhesion in CD44 KO cells, supporting our hypothesis that an abundance of integrin ligands on stiff HA hydrogels can compensate for the absence of CD44-based adhesions.

CD44-Mediated Signaling is Important for U-87 Migration on Stiff HA Hydrogels. We next explored the relative roles of HA hydrogel stiffness and RGD density on 2D cell migration. We used time-lapse microscopy to track cell speed on our HA array platform 6 hours after seeding. Increasing stiffness and/or RGD density increased cell migration speed across all cell lines (Figure 6C and Figure S9). However, CD44 KO cells generally migrated more slowly than nontargeting cells for a given matrix modulus and RGD concentration. On the softest gels, increasing RGD density rescued migration of CD44 KO cells relative to nontargeting cells (Figure 6D). Interestingly, CD44 KO cells migrated more slowly than nontargeting cells on the stiffest hydrogels across all RGD densities tested. These findings suggest a role for CD44 in facilitating cell migration on stiff HA hydrogels, even when ample integrin ligand is present.

DISCUSSION

We have developed a multiwell 2D hydrogel array platform that allows parallel culture and analysis of cells on various combinations of matrix stiffness and adhesivity. We successfully incorporated orthogonal stiffness and ligand density gradients on the array by programmable UV photopatterning. Proof-of-principle studies with hMSCs validated that the platform can recapitulate expected stiffness- and ligand density-sensitivity of YAP localization and spreading. We further applied the platform

https://doi.org/10.1021/acsbiomaterials.1c00065
ACS Biomater. Sci. Eng. 2021, 7, 2453−2465

to reveal context-dependent contributions of CD44 on GBM cell spreading, adhesion, and migration.

A common approach to developing multiwell hydrogel array platforms has been to fabricate hydrogel precursors directly within wells and then cross-link them in situ.[32−34] Hydrogels may also be cross-linked outside of the multiwell plates, cut into desired shapes, and later affixed to the multiwell plate.[55,56] Although these approaches have proven enormously valuable, it can be challenging to use these methods to vary multiple gel parameters in a single plate, since each gel must be individually fabricated. Our system provides an alternative approach that involves fabricating the gel array initially on a glass coverslip and then taping the substrate to a bottomless well plate. This aspect of our platform shares some conceptual connections with a previous PDMS screening platform in which various micro- and nanotopographies were presented in a standard multiwell format.[57] An important innovation of our approach is the use of laser-cut double-sided tape to both pattern the array and anchor the multiwell chamber to the device floor. Importantly, the laser-cut pattern is fully customizable and can accommodate hydrogel arrays of arbitrary dimensions and shapes depending on the multiwell plate format used. The platform also highlights the application of a programmable LAVA device, which allows for more precise tuning of photopatterning conditions than photomasks, as UV intensity and exposure time can be adjusted in a continuous manner.[41,42] Further, LEDs on the LAVA device are expected to produce extremely consistent intensity from one use to another, maximize adsorption efficiency and reduce batch-to-batch variation of stiffness patterning compared to traditional broad-spectrum UV light sources.

The array platform captured the synergic effect of ECM stiffness and RGD peptide density on hMSC spreading and YAP localization. In addition, our observation that YAP localization is insensitive to stiffness (12−48 kPa) on low RGD gels echoes recent reports that YAP localization was insensitive to stiffness at very high or low fibronectin density,[49] as both ligand density and stiffness induce YAP translocation to cytoskeletal tension and $\alpha V\beta 3$-integrin adhesion through similar mechanisms. For similar reasons, YAP localization is insensitive to ligand density on very stiff gels (91 kPa). Interestingly, YAP nuc/cyt ratio and hMSC area did not follow a normal distribution but resembled long-tail distributions. Even on hydrogels with the highest stiffness and ligand density, there is a subpopulation of hMSCs that favors cytoplasmic localization of YAP or is not well spread. Also, a small percentage of cells on soft, low RGD density gels are still capable of spreading or have nuclear YAP localization. The non-normal distribution may reflect intrinsic heterogeneities within the hMSC population, as has been observed elsewhere.[58]

This study also provides insight into the role of CD44 in U-87 cell spreading, adhesion, and motility. Although both CD44 KO and nontargeting U-87 cells appeared sensitive to matrix stiffness and RGD density on our HA gel array, CD44 KO cells were generally less spread and less strongly adhered than nontargeting cells. As expected, the deficiency of CD44 KO cells was exacerbated on gels with the lowest modulus and RGD density. However, increasing RGD density and/or stiffness generally restored cell spreading and adhesion to that of nontargeting cells. Interestingly, on soft matrices with high RGD density, CD44 KO cells displayed decreased adhesion strength to HA-hydrogels despite a classical "spread" 2D morphology. Previous studies have demonstrated that CD44 can complement and potentiate signaling from other surface receptors, including RGD-specific integrins, to drive cell spreading.[59,60] In this study, CD44 KO cells displayed decreased adhesion on soft matrices regardless of RGD density, highlighting the importance of both CD44- and integrin-based adhesions in particular matrix conditions.

Although cell migration speeds on our HA gel array generally increased with increasing hydrogel stiffness and RGD density, gel conditions facilitating the highest cell adhesion did not support the fastest cell migration. These results are consistent with the well-known biphasic dependence of cell migration on the strength of adhesion to the surrounding ECM.[61,62] Furthermore, a previous study demonstrated a biphasic relationship between CD44 protein expression and cell migration rates, with intermediate CD44 expression leading to the fastest overall motility in cell culture and poorest survival in human GBM.[63] On our platform, CD44 KO cells generally exhibited slower migration speeds than nontargeting cells across gel conditions. However, increasing RGD density restored migration speeds of CD44 KO cells to that of nontargeting cells on the softest gels, but not on the stiffest gels. Previous work from our laboratory has demonstrated that CD44 is sufficient to drive the formation of tension-bearing protrusions (microtentacles) that enable motility in the absence of integrin ligands.[44] Using our HA array platform, we found that CD44 is required to effectively migrate on stiff substrates, further highlighting the importance of CD44-HA interactions in the generation of cellular tension. Thus, the role of CD44 in cellular mechanosensing appears to be context-dependent; on soft HA matrices, CD44 is particularly important for cell adhesion and on stiff HA matrices it is important for cell migration.

One surprising result from our study is that although gels in our platform were permissive of hMSC osteogenic and adipogenic differentiation, we did not observe an appreciable matrix-dependent bias in lineage commitment. There are a number of potential explanations for this result. First, the soluble factors in the induction medium may have overridden the effects of matrix stiffness and thus induced significant adipogenesis on conditions as stiff as 91 kPa. We expect that a more comprehensive consideration of adhesive ligands and media formulation would produce a regime in which one sees stiffness-dependent hMSC differentiation. Second, despite seeding identical numbers of cells on each gel, we could not control cell density and cell clustering throughout the course of the experiment. For example, stiff gels routinely resulted in ∼20% higher cell density on day 7 of differentiation, presumably due to greater proliferation and/or increased attachment on these gels. High cell density, which is expected to reduce average cell area and promote adipogenesis,[64,65] may therefore have partially rescued adipogenesis on stiff gels. Third, the softest hydrogels in this study (12 kPa) may still be too stiff to significantly suppress osteogenesis or stimulate adipogenesis. Previous reports on various hydrogel platforms suggested an optimal modulus range for adipogenesis from several hundred pascals to 5 kPa.[22,29,34] The lowest stiffness (12 kPa) in our study was based on a DTT to HA monomer ratio of 0.15, and a lower ratio of DTT cross-linker may cause gel swelling and compromise cell imaging qualities. However, the "base" gel stiffness may be further reduced by optimizing gel composition, HA degree of functionalization, or cross-linker types. Lastly, the broad distributions of hMSC phenotypes for a given matrix condition may reflect intrinsic heterogeneities within the hMSC population. The lack of an expected stiffness-dependence differentiation on the gel array platform could be a consequence

https://doi.org/10.1021/acsbiomaterials.1c00065
ACS Biomater. Sci. Eng. 2021, 7, 2453−2465

of the heterogeneity that exists between MSC donors, tissue sources, culture methods, and even individual cells.[58]

The fabrication process of the array platform has significant room for further optimization. For example, the RGD density gradient in this system was achieved by manually mixing HA and RGD in various ratios, which may become prohibitively labor-intensive for highly parallelized arrays. This limitation could be addressed in the future by adapting dual photopatterning as described previously,[22,23,25] where the ECM ligand is conjugated to the backbone by photoreaction. An additional area with room for improvement is greater compatibility with dynamic, high-resolution imaging modalities. While we successfully measured cell migration speeds using low-magnification phase-contrast live imaging, higher-magnification imaging with shorter-working-distance objectives would likely require a thinner cover glass and/or thinner double-sided tape.

Despite these limitations, we envision that our platform could be adapted to a wide range of materials and applications beyond HA-based hydrogels since this platform could in principle accommodate any hydrogel formulation that can be affixed to glass, such as polyacrylamide- and poly(ethylene-glycol) (PEG)-based hydrogels. Moreover, combinatorial gradients of additional cell adhesion ligands and other ECM parameters (e.g., viscoelasticity, topography) could also potentially be incorporated to the platform through judicious choice of materials and photopatterning strategy. Changing the hydrogel composition, degree of functionalization, and cross-linking modalities may further extend the upper and lower limits of hydrogel stiffness. Finally, we anticipate that our system could bear value for mechanistic discovery and drug screening where mulitple matrix-based parameters are expected to cooperatively influence cell phenotype.

CONCLUSIONS

We have developed a combinatorial HA-based hydrogel array in a standard multiwell plate format, with orthogonal gradients of matrix elasticity and adhesive ligand density. On the array, cell spreading and YAP localization strongly respond to both matrix stiffness and RGD peptide density. Our array platform also reveals a context-dependent role of CD44 in GBM cell mechanosensitive behavior. The deployment of ECM-mimetic hydrogels in a familiar, user-friendly, and parallelized format should facilitate mechanistic discovery and screening applications.

ASSOCIATED CONTENT

Supporting Information

The Supporting Information is available free of charge at https://pubs.acs.org/doi/10.1021/acsbiomaterials.1c00065.

Me-HA reaction scheme and ^{1}H NMR spectrum, acrylic mold fabrication, dye leakage experiment, elastic modulus comparison of RGD-modified and unmodified HA hydrogels, digitally magnified YAP localization images, hMSC adipogenesis and osteogenesis characterization, U-87 cell spreading quantification, U-87 centrifugal adhesion quantification, U-87 2D random migration quantification (PDF)

AUTHOR INFORMATION

Corresponding Author

Sanjay Kumar − *Department of Bioengineering, Stanley Hall and Department of Chemical and Biomolecular Engineering, Gilman Hall, University of California, Berkeley, Berkeley, California 94720, United States; University of California, Berkeley − University of California, San Francisco Graduate Program in Bioengineering, Berkeley, California 94720, United States; Department of Bioengineering and Therapeutic Sciences, Byers Hall, University of California, San Francisco, San Francisco, California 94143, United States;* orcid.org/0000-0002-9996-4883; Email: skumar@berkeley.edu

Authors

Ruoxing Lei − *Department of Chemistry, Latimer Hall and Department of Bioengineering, Stanley Hall, University of California, Berkeley, Berkeley, California 94720, United States*

Erin A. Akins − *Department of Bioengineering, Stanley Hall, University of California, Berkeley, Berkeley, California 94720, United States; University of California, Berkeley − University of California, San Francisco Graduate Program in Bioengineering, Berkeley, California 94720, United States;* orcid.org/0000-0002-5359-5891

Kelly C. Y. Wong − *Department of Bioengineering, Stanley Hall, University of California, Berkeley, Berkeley, California 94720, United States*

Nicole A. Repina − *Department of Bioengineering, Stanley Hall, University of California, Berkeley, Berkeley, California 94720, United States; University of California, Berkeley − University of California, San Francisco Graduate Program in Bioengineering, Berkeley, California 94720, United States*

Kayla J. Wolf − *Department of Bioengineering, Stanley Hall, University of California, Berkeley, Berkeley, California 94720, United States; University of California, Berkeley − University of California, San Francisco Graduate Program in Bioengineering, Berkeley, California 94720, United States*

Garrett E. Dempsey − *Department of Nutritional Sciences and Toxicology, Morgan Hall, University of California, Berkeley, California 94720, United States*

David V. Schaffer − *Department of Bioengineering, Stanley Hall and Department of Chemical and Biomolecular Engineering, Gilman Hall, University of California, Berkeley, Berkeley, California 94720, United States; University of California, Berkeley − University of California, San Francisco Graduate Program in Bioengineering, Berkeley, California 94720, United States; Department of Molecular and Cell Biology, Life Sciences Addition, University of California, Berkeley, California 94720, United States;* orcid.org/0000-0002-9625-0121

Andreas Stahl − *University of California, Berkeley − University of California, San Francisco Graduate Program in Bioengineering, Berkeley, California 94720, United States; Department of Nutritional Sciences and Toxicology, Morgan Hall, University of California, Berkeley, California 94720, United States*

Complete contact information is available at: https://pubs.acs.org/10.1021/acsbiomaterials.1c00065

Funding

This work was supported by awards from the National Institutes of Health (R01GM122375, R01CA227136, and R01CA260443 to S.K., R01NS074831 to S.K. and D.V.S., and R01DK118940 to A.S. and S.K.) and the National Science Foundation (Graduate Research Fellowship to E.A.A.).

Notes

The authors declare no competing financial interest.

REFERENCES

(1) Vining, K. H.; Mooney, D. J. Mechanical forces direct stem cell behaviour in development and regeneration. *Nat. Rev. Mol. Cell Biol.* **2017**, *18*, 728−742.

(2) Wei, S. C.; Yang, J. Forcing through Tumor Metastasis: The Interplay between Tissue Rigidity and Epithelial-Mesenchymal Transition. *Trends Cell Biol.* **2016**, *26*, 111−120.

(3) Chen, J.; Kumar, S. Biophysical Regulation of Cancer Stem/Initiating Cells: Implications for disease mechanisms and translation. *Curr. Opin. Biomed. Eng.* **2017**, *1*, 87−95.

(4) Upadhyaya, A. Mechanosensing in the immune response. *Semin. Cell Dev. Biol.* **2017**, *71*, 137−145.

(5) Engler, A.; Bacakova, L.; Newman, C.; Hategan, A.; Griffin, M.; Discher, D. Substrate compliance versus ligand density in cell on gel responses. *Biophys. J.* **2004**, *86*, 617−628.

(6) Gong, Z.; Szczesny, S. E.; Caliari, S. R.; Charrier, E. E.; Chaudhuri, O.; Cao, X.; Lin, Y.; Mauck, R. L.; Janmey, P. A.; Burdick, J. A.; Shenoy, V. B. Matching material and cellular timescales maximizes cell spreading on viscoelastic substrates. *Proc. Natl. Acad. Sci. U. S. A.* **2018**, *115*, E2686−E2695.

(7) Zhou, Q.; Ge, L.; Guimarães, C. F.; Kühn, P. T.; Yang, L.; van Rijn, P. Development of a Novel Orthogonal Double Gradient for High-Throughput Screening of Mesenchymal Stem Cells-Materials Interaction. *Adv. Mater. Interfaces* **2018**, *5*, 1800504.

(8) Hou, Y.; Yu, L.; Xie, W.; Camacho, L. C.; Zhang, M.; Chu, Z.; Wei, Q.; Haag, R. Surface Roughness and Substrate Stiffness Synergize To Drive Cellular Mechanoresponse. *Nano Lett.* **2020**, *20*, 748−757.

(9) Darnell, M.; Gu, L.; Mooney, D. RNA-seq reveals diverse effects of substrate stiffness on mesenchymal stem cells. *Biomaterials* **2018**, *181*, 182−188.

(10) Liu, X.; Liu, R.; Gu, Y.; Ding, J. Nonmonotonic Self-Deformation of Cell Nuclei on Topological Surfaces with Micropillar Array. *ACS Appl. Mater. Interfaces* **2017**, *9*, 18521−18530.

(11) Geckil, H.; Xu, F.; Zhang, X.; Moon, S.; Demirci, U. Engineering hydrogels as extracellular matrix mimics. *Nanomedicine (London, U. K.)* **2010**, *5*, 469−484.

(12) Zhu, J.; Marchant, R. E. Design properties of hydrogel tissue-engineering scaffolds. *Expert Rev. Med. Devices* **2011**, *8*, 607−626.

(13) Kyburz, K. A.; Anseth, K. S. Synthetic mimics of the extracellular matrix: how simple is complex enough? *Ann. Biomed. Eng.* **2015**, *43*, 489−500.

(14) Xing, H.; Lee, H.; Luo, L.; Kyriakides, T. R. Extracellular matrix-derived biomaterials in engineering cell function. *Biotechnol. Adv.* **2020**, *42*, 107421.

(15) Huebsch, N.; Arany, P. R.; Mao, A. S.; Shvartsman, D.; Ali, O. A.; Bencherif, S. A.; Rivera-Feliciano, J.; Mooney, D. J. Harnessing traction-mediated manipulation of the cell/matrix interface to control stem-cell fate. *Nat. Mater.* **2010**, *9*, 518−526.

(16) Chaudhuri, O.; Gu, L.; Klumpers, D.; Darnell, M.; Bencherif, S. A.; Weaver, J. C.; Huebsch, N.; Lee, H.-P.; Lippens, E.; Duda, G. N.; Mooney, D. J. Hydrogels with tunable stress relaxation regulate stem cell fate and activity. *Nat. Mater.* **2016**, *15*, 326−334.

(17) Xia, T.; Liu, W.; Yang, L. A review of gradient stiffness hydrogels used in tissue engineering and regenerative medicine. *J. Biomed. Mater. Res., Part A* **2017**, *105*, 1799−1812.

(18) Rowlands, A. S.; George, P. A.; Cooper-White, J. J. Directing osteogenic and myogenic differentiation of MSCs: interplay of stiffness and adhesive ligand presentation. *Am. J. Physiol. Cell Physiol.* **2008**, *295*, C1037−44.

(19) Kilian, K. A.; Mrksich, M. Directing Stem Cell Fate by Controlling the Affinity and Density of Ligand-Receptor Interactions at the Biomaterials Interface. *Angew. Chem., Int. Ed.* **2012**, *51*, 4891−4895.

(20) Wilson, M. J.; Jiang, Y.; Yañez-Soto, B.; Liliensiek, S.; Murphy, W. L.; Nealey, P. F. Arrays of topographically and peptide-functionalized hydrogels for analysis of biomimetic extracellular matrix properties. *J. Vac. Sci. Technol., B: Nanotechnol. Microelectron.: Mater., Process., Meas., Phenom.* **2012**, *30*, 06F903.

(21) Guo, Z.; Hu, K.; Sun, J.; Zhang, T.; Zhang, Q.; Song, L.; Zhang, X.; Gu, N. Fabrication of Hydrogel with Cell Adhesive Micropatterns for Mimicking the Oriented Tumor-Associated Extracellular Matrix. *ACS Appl. Mater. Interfaces* **2014**, *6*, 10963−10968.

(22) Rape, A. D.; Zibinsky, M.; Murthy, N.; Kumar, S. A synthetic hydrogel for the high-throughput study of cell-ECM interactions. *Nat. Commun.* **2015**, *6*, 8129.

(23) Tong, X.; Jiang, J.; Zhu, D.; Yang, F. Hydrogels with Dual Gradients of Mechanical and Biochemical Cues for Deciphering Cell-Niche Interactions. *ACS Biomater. Sci. Eng.* **2016**, *2*, 845−852.

(24) Hansen, T. D.; Koepsel, J. T.; Le, N. N.; Nguyen, E. H.; Zorn, S.; Parlato, M.; Loveland, S. G.; Schwartz, M. P.; Murphy, W. L. Biomaterial arrays with defined adhesion ligand densities and matrix stiffness identify distinct phenotypes for tumorigenic and non-tumorigenic human mesenchymal cell types. *Biomater. Sci.* **2014**, *2*, 745−756.

(25) Vega, S. L.; Kwon, M. Y.; Song, K. H.; Wang, C.; Mauck, R. L.; Han, L.; Burdick, J. A. Combinatorial hydrogels with biochemical gradients for screening 3D cellular microenvironments. *Nat. Commun.* **2018**, *9*, 614.

(26) Ma, Y.; Policastro, G. M.; Li, Q.; Zheng, J.; Jacquet, R.; Landis, W. J.; Becker, M. L. Concentration-Dependent hMSC Differentiation on Orthogonal Concentration Gradients of GRGDS and BMP-2 Peptides. *Biomacromolecules* **2016**, *17*, 1486−1495.

(27) Guermani, E.; Shaki, H.; Mohanty, S.; Mehrali, M.; Arpanaei, A.; Gaharwar, A. K.; Dolatshahi-Pirouz, A. Engineering complex tissue-like microgel arrays for evaluating stem cell differentiation. *Sci. Rep.* **2016**, *6*, 30445.

(28) Richardson, T. C.; Mathew, S.; Candiello, J. E.; Goh, S. K.; Kumta, P. N.; Banerjee, I. Development of an Alginate Array Platform to Decouple the Effect of Multiparametric Perturbations on Human Pluripotent Stem Cells During Pancreatic Differentiation. *Biotechnol. J.* **2018**, *13*, 1700099.

(29) Hadden, W. J.; Young, J. L.; Holle, A. W.; McFetridge, M. L.; Kim, D. Y.; Wijesinghe, P.; Taylor-Weiner, H.; Wen, J. H.; Lee, A. R.; Bieback, K.; Vo, B.-N.; Sampson, D. D.; Kennedy, B. F.; Spatz, J. P.; Engler, A. J.; Choi, Y. S. Stem cell migration and mechanotransduction on linear stiffness gradient hydrogels. *Proc. Natl. Acad. Sci. U. S. A.* **2017**, *114*, 5647−5652.

(30) Dolatshahi-Pirouz, A.; Nikkhah, M.; Gaharwar, A. K.; Hashmi, B.; Guermani, E.; Aliabadi, H.; Camci-Unal, G.; Ferrante, T.; Foss, M.; Ingber, D. E.; Khademhosseini, A. A combinatorial cell-laden gel microarray for inducing osteogenic differentiation of human mesenchymal stem cells. *Sci. Rep.* **2015**, *4*, 3896.

(31) Ranga, A.; Gobaa, S.; Okawa, Y.; Mosiewicz, K.; Negro, A.; Lutolf, M. P. 3D niche microarrays for systems-level analyses of cell fate. *Nat. Commun.* **2014**, *5*, 4324.

(32) Mih, J. D.; Sharif, A. S.; Liu, F.; Marinkovic, A.; Symer, M. M.; Tschumperlin, D. J. A multiwell platform for studying stiffness-dependent cell biology. *PLoS One* **2011**, *6*, e19929.

(33) Díaz-Bello, B.; Monroy-Romero, A. X.; Pérez-Calixto, D.; Zamarrón-Hernández, D.; Serna-Marquez, N.; Vázquez-Victorio, G.; Hautefeuille, M. Method for the Direct Fabrication of Polyacrylamide Hydrogels with Controlled Stiffness in Polystyrene Multiwell Plates for Mechanobiology Assays. *ACS Biomater. Sci. Eng.* **2019**, *5*, 4219−4227.

(34) Hribar, K. C.; Buckley, P. Apparatus for patterning hydrogels into multi-well plates. Patent US 20180011408 A1, 2018.

(35) Highley, C. B.; Prestwich, G. D.; Burdick, J. A. Recent advances in hyaluronic acid hydrogels for biomedical applications. *Curr. Opin. Biotechnol.* **2016**, *40*, 35−40.

(36) Wolf, K. J.; Kumar, S. Hyaluronic Acid: Incorporating the Bio into the Material. *ACS Biomater. Sci. Eng.* **2019**, *5*, 3753−3765.

(37) Ananthanarayanan, B.; Kim, Y.; Kumar, S. Elucidating the mechanobiology of malignant brain tumors using a brain matrix-mimetic hyaluronic acid hydrogel platform. *Biomaterials* **2011**, *32*, 7913−7923.

(38) Kim, Y.; Kumar, S. CD44-mediated adhesion to hyaluronic acid contributes to mechanosensing and invasive motility. *Mol. Cancer Res.* **2014**, *12*, 1416−1429.

https://doi.org/10.1021/acsbiomaterials.1c00065
ACS Biomater. Sci. Eng. 2021, 7, 2453−2465

(39) Kim, I. L.; Khetan, S.; Baker, B. M.; Chen, C. S.; Burdick, J. A. Fibrous hyaluronic acid hydrogels that direct MSC chondrogenesis through mechanical and adhesive cues. *Biomaterials* **2013**, *34*, 5571−5580.
(40) Cosgrove, B. D.; Mui, K. L.; Driscoll, T. P.; Caliari, S. R.; Mehta, K. D.; Assoian, R. K.; Burdick, J. A.; Mauck, R. L. N-cadherin adhesive interactions modulate matrix mechanosensing and fate commitment of mesenchymal stem cells. *Nat. Mater.* **2016**, *15*, 1297−1306.
(41) Repina, N. A.; McClave, T.; Johnson, H. J.; Bao, X.; Kane, R. S.; Schaffer, D. V. Engineered Illumination Devices for Optogenetic Control of Cellular Signaling Dynamics. *Cell Rep.* **2020**, *31*, 107737.
(42) Repina, N. A.; Johnson, H. J.; McClave, T.; Kane, R. S.; Schaffer, D. V. Protocol to Fabricate Engineered Illumination Devices for Optogenetic Control of Cellular Signaling Dynamics. *STAR Protoc.* **2020**, *1*, 100141.
(43) MacKay, J. L.; Kumar, S. Measuring the Elastic Properties of Living Cells with Atomic Force Microscopy Indentation. In *Cell Imaging Techniques*; Taatjes, D. J., Roth, J., Eds.; Methods in Molecular Biology; Humana Press: Totowa, NJ, 2013; pp 313−329.
(44) Wolf, K. J.; Shukla, P.; Springer, K.; Lee, S.; Coombes, J. D.; Choy, C. J.; Kenny, S. J.; Xu, K.; Kumar, S. A mode of cell adhesion and migration facilitated by CD44-dependent microtentacles. *Proc. Natl. Acad. Sci. U. S. A.* **2020**, *117*, 11432.
(45) Engler, A. J.; Sen, S.; Sweeney, H. L.; Discher, D. E. Matrix Elasticity Directs Stem Cell Lineage Specification. *Cell* **2006**, *126*, 677−689.
(46) Nemir, S.; West, J. L. Synthetic materials in the study of cell response to substrate rigidity. *Ann. Biomed. Eng.* **2010**, *38*, 2−20.
(47) Dupont, S.; Morsut, L.; Aragona, M.; Enzo, E.; Giulitti, S.; Cordenonsi, M.; Zanconato, F.; Le Digabel, J.; Forcato, M.; Bicciato, S.; Elvassore, N.; Piccolo, S. Role of YAP/TAZ in mechanotransduction. *Nature* **2011**, *474*, 179−184.
(48) Das, A.; Fischer, R. S.; Pan, D.; Waterman, C. M. YAP nuclear localization in the absence of cell-cell contact is mediated by a filamentous actin-dependent, Myosin IIand Phospho-YAP-independent pathway during extracellular matrix mechanosensing. *J. Biol. Chem.* **2016**, *291*, 6096−6110.
(49) Stanton, A. E.; Tong, X.; Lee, S.; Yang, F. Biochemical Ligand Density Regulates Yes-Associated Protein Translocation in Stem Cells through Cytoskeletal Tension and Integrins. *ACS Appl. Mater. Interfaces* **2019**, *11*, 8849−8857.
(50) Park, J. S.; Chu, J. S.; Tsou, A. D.; Diop, R.; Tang, Z.; Wang, A.; Li, S. The effect of matrix stiffness on the differentiation of mesenchymal stem cells in response to TGF-β. *Biomaterials* **2011**, *32*, 3921−3930.
(51) Lee, J. P.; Kassianidou, E.; MacDonald, J. I.; Francis, M. B.; Kumar, S. N-terminal specific conjugation of extracellular matrix proteins to 2-pyridinecarboxaldehyde functionalized polyacrylamide hydrogels. *Biomaterials* **2016**, *102*, 268−276.
(52) Zhao, W.; Li, X.; Liu, X.; Zhang, N.; Wen, X. Effects of substrate stiffness on adipogenic and osteogenic differentiation of human mesenchymal stem cells. *Mater. Sci. Eng., C* **2014**, *40*, 316−323.
(53) Ye, K.; Wang, X.; Cao, L.; Li, S.; Li, Z.; Yu, L.; Ding, J. Matrix Stiffness and Nanoscale Spatial Organization of Cell-Adhesive Ligands Direct Stem Cell Fate. *Nano Lett.* **2015**, *15*, 4720−4729.
(54) Lee, J.; Abdeen, A. A.; Tang, X.; Saif, T. A.; Kilian, K. A. Matrix directed adipogenesis and neurogenesis of mesenchymal stem cells derived from adipose tissue and bone marrow. *Acta Biomater.* **2016**, *42*, 46−55.
(55) Semler, E. J.; Lancin, P. A.; Dasgupta, A.; Moghe, P. V. Engineering hepatocellular morphogenesis and function via ligand-presenting hydrogels with graded mechanical compliance. *Biotechnol. Bioeng.* **2005**, *89*, 296−307.
(56) Syed, S.; Karadaghy, A.; Zustiak, S. Simple polyacrylamide-based multiwell stiffness assay for the study of stiffness-dependent cell responses. *J. Visualized Exp.* **2015**, *2015*, 1−12.
(57) Hu, J.; Gondarenko, A. A.; Dang, A. P.; Bashour, K. T.; O'Connor, R. S.; Lee, S.; Liapis, A.; Ghassemi, S.; Milone, M. C.; Sheetz, M. P.; Dustin, M. L.; Kam, L. C.; Hone, J. C. High-Throughput Mechanobiology Screening Platform Using Micro- and Nanotopography. *Nano Lett.* **2016**, *16*, 2198−2204.
(58) Wilson, A.; Hodgson-Garms, M.; Frith, J. E.; Genever, P. Multiplicity of mesenchymal stromal cells: Finding the right route to therapy. *Front. Immunol.* **2019**, *10*, 1−8.
(59) Chopra, A.; Murray, M. E.; Byfield, F. J.; Mendez, M. G.; Halleluyan, R.; Restle, D. J.; Raz-Ben Aroush, D.; Galie, P. A.; Pogoda, K.; Bucki, R.; Marcinkiewicz, C.; Prestwich, G. D.; Zarembinski, T. I.; Chen, C. S.; Puré, E.; Kresh, J. Y.; Janmey, P. A. Augmentation of integrin-mediated mechanotransduction by hyaluronic acid. *Biomaterials* **2014**, *35*, 71−82.
(60) Mandal, K.; Raz-Ben Aroush, D.; Graber, Z. T.; Wu, B.; Park, C. Y.; Fredberg, J. J.; Guo, W.; Baumgart, T.; Janmey, P. A. Soft Hyaluronic Gels Promote Cell Spreading, Stress Fibers, Focal Adhesion, and Membrane Tension by Phosphoinositide Signaling, Not Traction Force. *ACS Nano* **2019**, *13*, 203−214.
(61) Palecek, S. P.; Loftus, J. C.; Ginsberg, M. H.; Lauffenburger, D. A.; Horwitz, A. F. Integrin-ligand binding properties govern cell migration speed through cell-substratum adhesiveness [published erratum appears in Nature 1997 Jul 10;388(6638):210]. *Nature* **1997**, *385*, 537−540.
(62) Pathak, A.; Kumar, S. From molecular signal activation to locomotion: An integrated, multiscale analysis of cell motility on defined matrices. *PLoS One* **2011**, *6*, e18423.
(63) Klank, R. L.; Decker Grunke, S. A.; Bangasser, B. L.; Forster, C. L.; Price, M. A.; Odde, T. J.; SantaCruz, K. S.; Rosenfeld, S. S.; Canoll, P.; Turley, E. A.; McCarthy, J. B.; Ohlfest, J. R.; Odde, D. J. Biphasic Dependence of Glioma Survival and Cell Migration on CD44 Expression Level. *Cell Rep.* **2017**, *18*, 23−31.
(64) McBeath, R.; Pirone, D. M.; Nelson, C. M.; Bhadriraju, K.; Chen, C. S. Cell Shape, Cytoskeletal Tension, and RhoA Regulate Stem Cell Lineage Commitment. *Dev. Cell* **2004**, *6*, 483−495.
(65) Wiesner, M.; Berberich, O.; Hoefner, C.; Blunk, T.; Bauer-Kreisel, P. Gap junctional intercellular communication in adipose-derived stromal/stem cells is cell density-dependent and positively impacts adipogenic differentiation. *J. Cell. Physiol.* **2018**, *233*, 3315−3329.

https://doi.org/10.1021/acsbiomaterials.1c00065
ACS Biomater. Sci. Eng. 2021, 7, 2453−2465